PERGAMON

International Journal of Multiphase Flow 28 (2002) 51–67

International Journal of Multiphase Flow

www.elsevier.com/locate/ijmulflow

Experimental study of air–water countercurrent annular flow under post-flooding conditions

M. Vijayan, S. Jayanti *, A.R. Balakrishnan

Department of Chemical Engineering, Indian Institute of Technology, Chennai 600 036, India

Received 13 November 2000; received in revised form 30 August 2001

Abstract

Experiments have been conducted on countercurrent flow of air and water in tubes of 25, 67 and 99 mm diameter. Measurements of the pressure gradient, film thickness and down flow rate were made for a range of air and water flow rates under pre- and post-flooding conditions. The data showed that the pressure gradient did not increase appreciably until just before the onset of flooding. The mean film thickness under pre-flooding conditions was also predicted well by the falling film correlations. However, both quantities showed significant deviations from this pattern under post-flooding conditions. Existing correlations for predicting the pressure drop under post-flooding conditions gave poor prediction of the present data as well of the data from the literature. New correlations are presented for the pressure gradient and the mean film thickness under post-flooding conditions. © 2001 Published by Elsevier Science Ltd.

1. Introduction

Flooding is closely associated with the limit of stable countercurrent gas–liquid flow and as such it is an important design criterion in a variety of process equipment such as falling film absorbers, evaporators, heat pipes, reflux condensers and in some aspects of nuclear reactor safety. Although flooding has been studied for a number of decades, the focus has invariably been on the conditions at which flooding is initiated (Hewitt and Wallis, 1963; Clift et al., 1966; Pushkina and Sorokin, 1969; Alekseev et al., 1972) and, more recently, on the mechanism by which flooding takes place in countercurrent gas–liquid annular flow (McQuillan et al., 1985; Zabaras and Dukler, 1988; Govan et al., 1991; Jayanti et al., 1996; Vijayan et al.,

* Corresponding author. Tel.: +91-44-4458227; fax: +91-44-2350509.
E-mail address: sjayanti@iitm.ac.in (S. Jayanti).

0301-9322/02/$ - see front matter © 2001 Published by Elsevier Science Ltd.
PII: S0301-9322(01)00066-0

2001). There have been relatively few studies under post-flooding conditions. Bharathan et al. (1978) and Bharathan and Wallis (1983) presented a correlation for the calculation of the interfacial friction factor in countercurrent flow while Richter (1981) suggested a minor modification of the Wallis (1969) correlation for the friction factor in annular flow. Data of pressure gradient under post-flooding conditions were reported by Dukler and Smith (1982) while measurements of the down flow rate under post-flooding conditions were reported to a limited extent by Clift et al. (1966) and more recently by Zabaras and Dukler (1988) and Govan et al. (1991). Film thickness measurements under post-flooding conditions were also reported by Zabaras and Dukler (1988). However, development of correlations of these data has not been attempted to-date, except by Bharathan and co-workers in the case of the pressure gradient.

A systematic study of the effect of tube diameter on the mechanism of flooding has recently been undertaken by the present authors (Vijayan et al., 2001). As part of this study, the important parameters of countercurrent flow, namely, pressure gradient in the test section, down flow rate and film thickness have been measured over a range of flow conditions including pre- and post-flooding regimes in two test section diameters. These data, along with some of the results available in the literature, are used to develop correlations to predict the countercurrent flow parameters.

2. Experimental details

2.1. Flow circuit

The experimental set-up used in the present study is shown schematically in Fig. 1 and is the same as that used in earlier studies (Vijayan et al., 2001). It consists of three countercurrent flow columns having internal diameters of 25, 67 and 99 mm with common air and water connections. Air is fed to the test section from one of three air compressors (with maximum capacities of 8, 20 and 200 m^3/h at STP conditions) connected in series. A needle valve, located just before the entrance to each test section, is used for flow control. Water is pumped from a reservoir through a pre-filter and is fed into the test section by two pumps, each having a capacity of 0.5 hp, connected in series. A bypass circuit is provided to minimize the load on the pumps and to control the water flow rate under low flow rate conditions.

Each column is made of transparent acrylic plastic material and has a total length of 4 m. Water enters and exits from the test section through a filter assembly to provide smooth inlet and outlet conditions. The height of each column is 4 m; however, the length of test section, i.e., the height between the water inlet and the water outlet is 2.0 m for the 25 mm diameter test section and 1.8 m for 67 and 99 mm diameter test sections. There is thus about 1 m length of pipe each below and above the test section which serves to provide smooth inlet and outlet conditions for the air flow as well. Air and water, if any, leave the test section from the top through a PVC pipe and are separated in an open tank. Water is fed back to the main water tank by gravity. The pressure in each column could be controlled by a valve located in the PVC pipe.

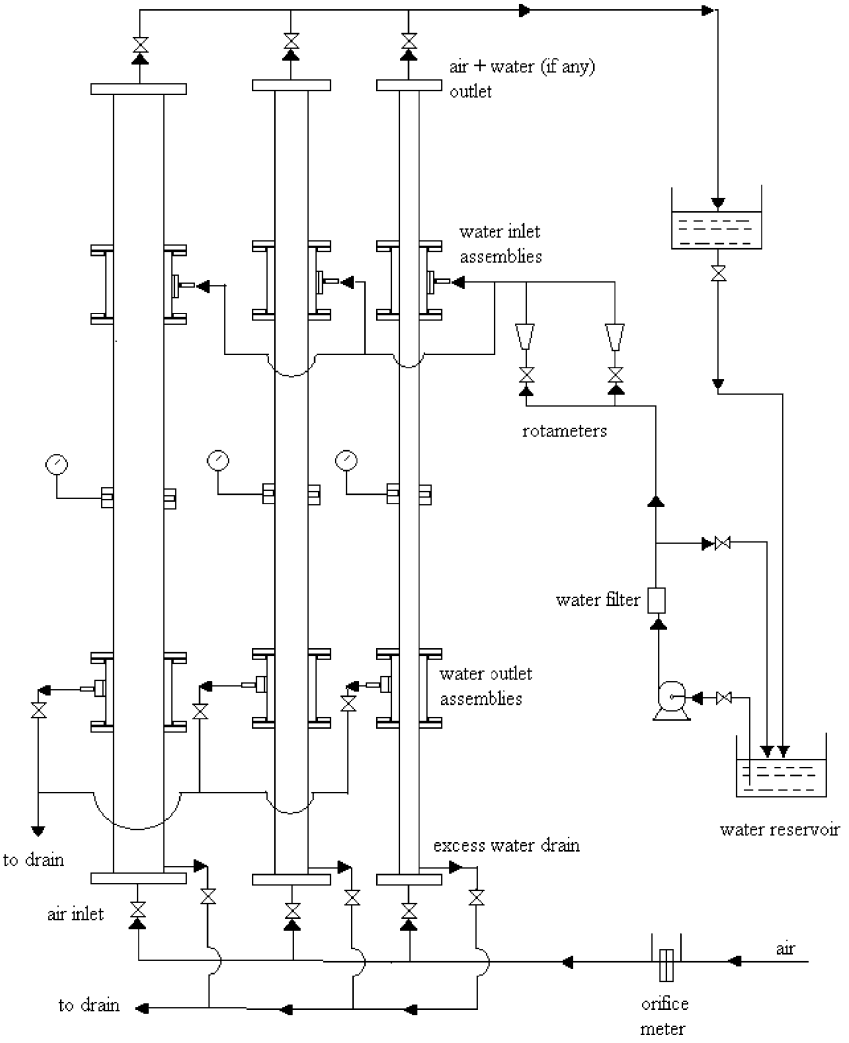

Fig. 1. Schematic diagram of the rig assembly showing the three test sections.

2.2. Instrumentation

The primary variables that were measured during the experiments were the pressure, the pressure drop, the input flow rate of each phase, the flow rate of water, if any, through the water outlet and the film thickness. Air and water flow rates into the test section were measured using an orifice meter and a bank of rotameters, respectively. The static pressure in the column was measured using a pressure gauge while the pressure drop was measured using water or mercury-filled manometers. The water flow rate through the top outlet, if any, was determined by collecting it in a measuring flask over a period of time. The temporal variation of the film thickness was measured using a two-pin type of conductance probe and is described in detail by Vijayan et al. (1999).

2.3. Experimental procedure

The above set-up was used to measure pressure drop and film thickness for a range of air and water flow rates through a given test section. In each run, the water flow rate was set at a specified level and the air flow rate was increased in small increments from a pure falling film case. After each increment in the air flow rate, the flow was allowed to settle for a few minutes and the flow rate of each phase, the pressure drop in the test section and the film thickness at three locations in the test section were recorded. The flow structure, e.g., presence of large waves, droplets, etc., was observed by the naked eye and recorded. The water flow rate through the top outlet, if any, was collected in a measuring flask over a period of time. After these measurements were over, the air flow rate was further increased by a small increment. These measurements and observations were made at several air flow rates right up to and beyond the point of flooding. The experiments were *not* conducted at constant inlet pressure condition, and the test section pressure was allowed to change from run to run, though the variation was small. The maximum test section pressure at the highest air flow rates for each water flow rate was typically of the order of 0.5 bar (gauge).

3. Results

The various phenomena that occur in countercurrent flow are best understood by studying the flow parameters as the air flow rate is increased in small steps while maintaining a constant inlet liquid flow rate. A typical set of results obtained in one such run in the 25 mm diameter tube is shown in Fig. 2(a). Here the water flow rate was set at 0.0278 kg/s and the air flow rate was varied over a wide range. The pressure gradient and the down flow rate of water are plotted as a function of the air flow rate. There were fairly small amplitude interfacial waves present when there was no air flow rate. As the air flow rate was increased, larger amplitude waves began to form and occasionally droplets were sheared away from it. The pressure gradient under these conditions (of onset of droplet entrainment) is very small. At slightly higher air flow rates, the rate of entrainment of droplets increased; however, these were confined to the bottom half of the test section and no droplets could be carried beyond the liquid inlet. At this point, large waves were formed occasionally but the pressure gradient remained very small. As the air flow rate was further increased, the distortion of the interface became more pronounced and the wave amplitude appeared to increase tremendously. However, the waves were not coherent circumferentially. The pressure drop at this point is higher but is still considerably lesser than that at flooding, which is defined here based on sudden and sustained increase in the pressure gradient in the test section. Just before flooding, large amplitude, ring-type waves were formed and the interface became highly dimpled. One notable feature here was the absence of droplets; in the 25 mm diameter tube, the droplet concentration remained very small right up to flooding. The pressure drop still remains low compared to that at flooding. At the flooding point, some of these large amplitude waves were carried up repeatedly and fairly periodically. The structure of the interface within this upward moving wave appeared to be chaotic with large amplitude waves. The pressure drop becomes very high. The flow structure in post-flooding conditions is typically characterized by

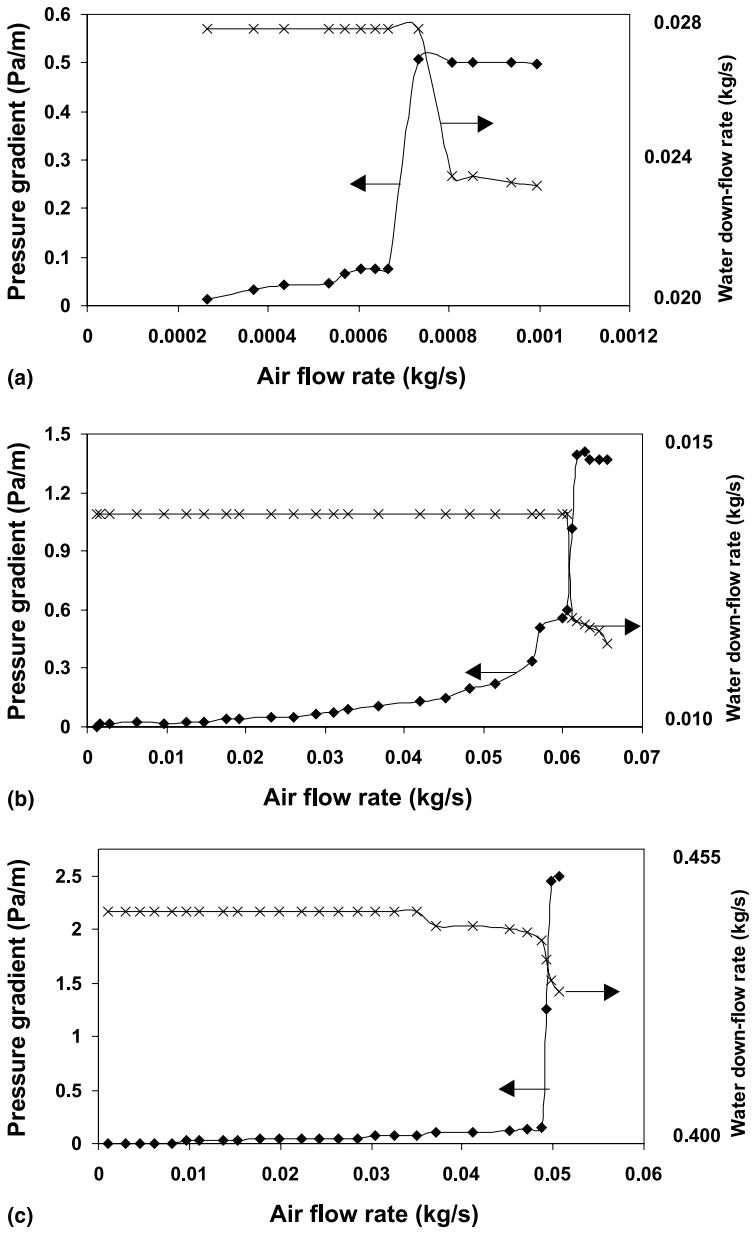

Fig. 2. Typical variation of the pressure gradient (diamonds) and the liquid down flow rate (crosses) in the (a) 25, (b) 67 and (c) 99 mm diameter test section.

considerable entrainment of bubbles in the liquid film. The pressure gradient remains very high though this is not higher than at flooding.

In the case of the 67 mm diameter tube, the interface, when there is no air flow, appears to be rougher than the corresponding one in the 25 mm diameter test section. As the air flow rate is

increased, large amplitude waves are formed from which droplets are torn off. This results in the formation of number of droplets of various sizes unlike in the case of 25 mm tube diameter where only a few droplets could be seen. The formation of big waves (large enough to lead to droplet entrainment) is confined initially to the bottom part of test section. However, droplets could be seen further up because some of these are carried away by the air stream. As the flooding air velocity is approached for a given water flow rate, larger waves are formed and some of these are taken up a short distance by the air stream. These then collapse to give rise to extensive droplet entrainment. This process of large wave generation, being carried up and breaking up is repeated continuously giving the appearance of churn-like flow of the liquid. Typically, the churning regime is confined to a small length of the tube. At higher air flow rates, the churning motion becomes more violent and may spread up the tube. This confined churn-like flow structure does not appear in the 25 mm diameter tube.

The pressure drop and the down flow rate in the test section measured in the 67 mm tube diameter are shown in Fig. 2(b) for a water flow rate of 0.111 kg/s. The pressure drop does not change appreciably as long as the air flow rate is insufficient to create the churn-like flow structure. Similarly, the down flow rate begins to decrease only after the formation of the churn-like region; any droplets carried away by the air stream constitute a very small part of the total liquid flow rate.

The situation in the 99 mm diameter tube is similar to that in the 67 mm tube. Because of the large diameter of the tube, churning motion could be created only in the case of the largest possible water flow rate of 0.444 kg/s. Here droplets were generated at fairly low air flow rates but large waves could be created only at much higher air flow rates. The flow structure in the churning zone at the highest air flow rate used in this test section is similar to that of the confined churning motion found in the 67 mm diameter tube prior to flooding. It appears likely that if higher water/air flow rates are used, more chaotic film flow throughout the column may also be achieved in the 99 mm diameter tube. The pressure drop in the test section and the down flow rate measured in the 99 mm diameter tube (Fig. 2(c)) show that the sudden increase in the pressure gradient and a sudden decrease in the down flow rate are possible only after a churn-like motion is created in the liquid film.

Typical variation of the mean film thickness is shown in Fig. 3 for the three tube diameters. It can be seen (Fig. 3(a)) that the mean film thickness does not change significantly until just before the flooding point. There is a sudden increase at the flooding point followed by a gradual decrease under post-flooding conditions. The increase in the mean film thickness at the flooding point is much more pronounced in the 25 mm diameter than in the 67 mm diameter tube (Fig. 3(b)), perhaps due to the formation of large-amplitude waves in the former near the liquid outlet (Vijayan et al., 2001). The results of Zabaras and Dukler (1988) in a 50.8 mm diameter tube are also similar and show a sudden increase in the mean film thickness at the flooding point. However, there is a faster decrease in the film thickness in the post-flooding regime. This may be due to the different post-flooding behaviour obtained for the down flow rate of the liquid in the two experiments. Zabaras and Dukler (1988) obtained a steady decrease in the down flow rate following flooding. Typical results obtained in the present experiments are shown in Fig. 4. Here the down flow rate remains constant until the flooding point and then decreases suddenly by about 20–30% and then levels off. This is in contrast to the results of Zabaras and Dukler (1988) who did not find such a sudden drop and reported that the flooding curve coincided with the down flow rate curve.

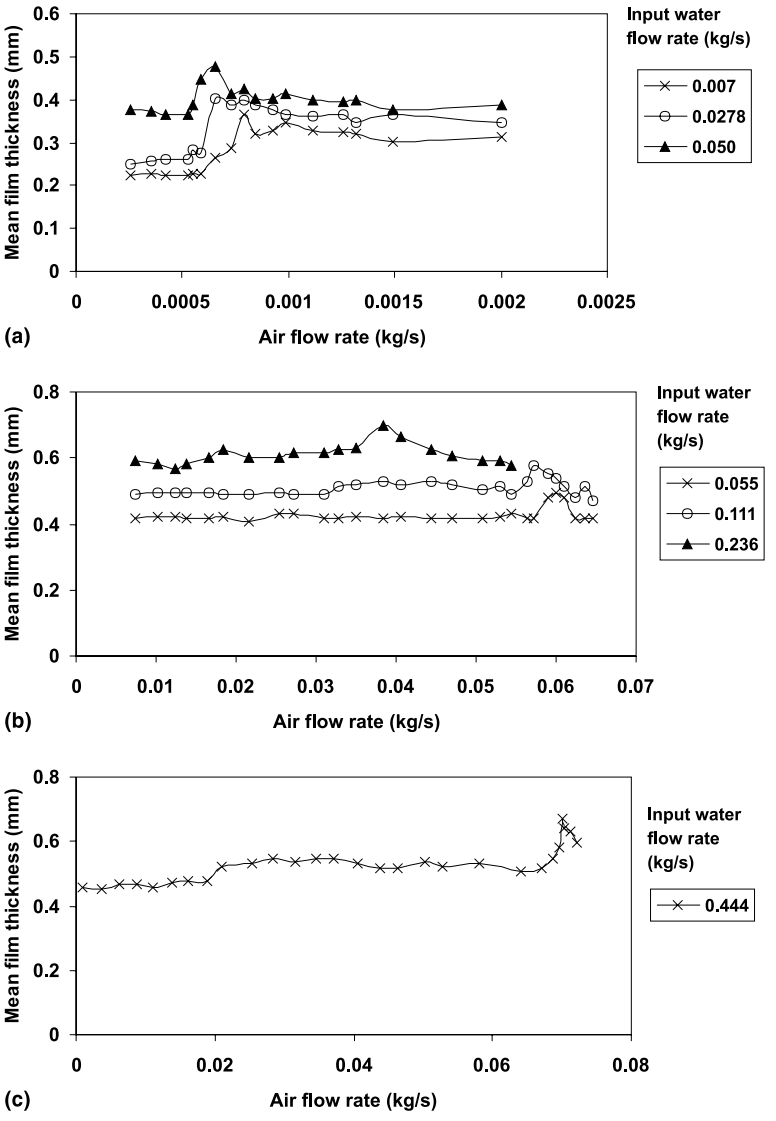

Fig. 3. Variation of the mean film thickness with air flow rate in (a) 25, (b) 67 and (c) 99 mm diameter test sections at various water input flow rates.

However, Clift et al. (1966) reported that in their experiments, the down flow rate dropped suddenly, following flooding, to a value which was sometimes as low as one-fifth of the pre-flooding flow rate. Govan et al. (1991) conducted experiments with a porous wall outlet in a 32 mm diameter tube and found that the down flow curve and the flooding curve were distinct at high liquid flow rates. However, at low liquid flow rates, the down flow curve lay above the flooding curve. This surprising result, namely, that the maximum down flow rate being more than the down flow rate at flooding, was attributed to the so-called "hanging film phenomenon" in which a liquid film exists above the liquid injector with no net upward flow of liquid. Any further

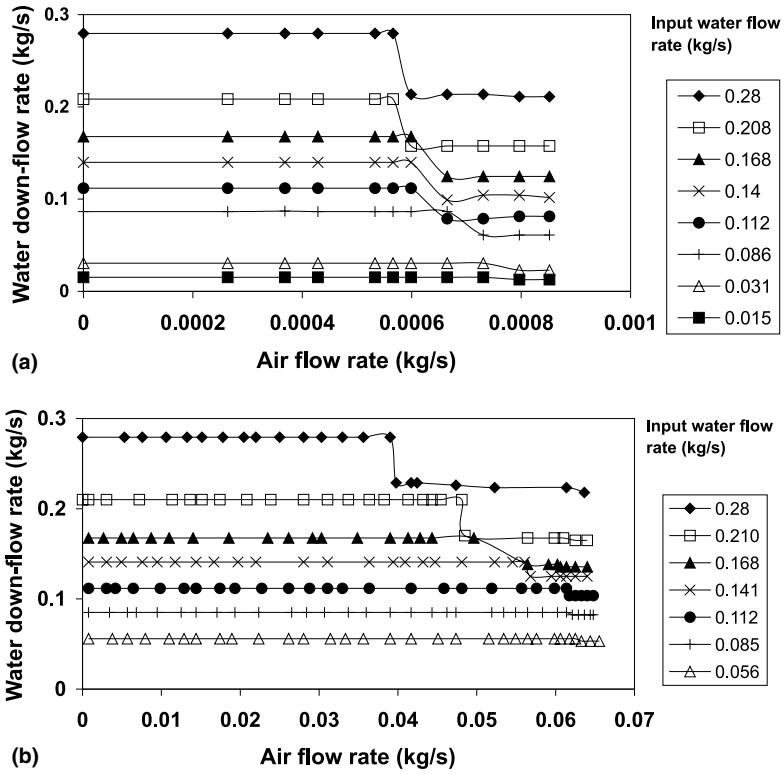

Fig. 4. Variation of water down flow rate with air flow rate in the post-flooding region in the (a) 25 mm and (b) 67 mm diameter test sections.

increase in the liquid or the air flow rate would result in a net outflow of liquid through the top outlet.

In view of these discrepancies and in view of the limited air flow rates available, an independent series of experiments were conducted in the 25 mm diameter tube to study the down flow rate variation with air flow rate right up to the point of tube dryout. The results are summarized in Fig. 5 where the liquid down flow rate under post-flooding conditions is plotted as a function of air flow rate for different liquid flow rates at the inlet. It can be seen that, in all the cases, there is a sudden drop in down flow rate immediately after flooding followed by a plateau region in which the down flow rate does not decrease with increasing air flow rate. At higher air flow rates, there is a gradual decrease in the liquid down flow rate until the tube dries out completely. These results indicate that the liquid film becomes "sub-critical" immediately after flooding and support the cryptic remark of Hewitt (1989) to the effect that the falling film region below the liquid injector under post-flooding conditions could be expected to behave in a manner analogous to a normal falling film with a sub-flooding gas velocity. However, the pressure gradient in the test section under these conditions remains high (at post-flooding levels) and the flow is not sub-critical from the point of view of pressure gradient. The liquid flow in the column is typically unstable and is indicative of large interfacial friction; however, further

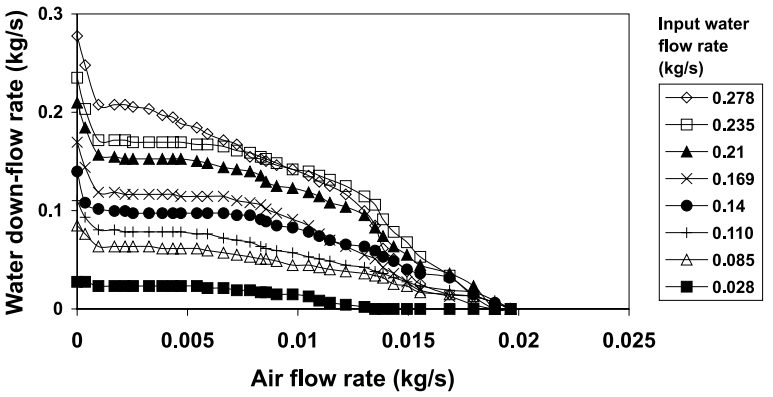

Fig. 5. Variation of the water down flow rate in the 25 mm tube diameter test section at high air flow rates.

decrease in the down flow rate was possible only after the gas flow rate was increased beyond a certain value.

This typical variation of down flow rate with air flow rate is shown schematically in Fig. 6(a). Here point A is the air flow rate at which flooding occurs and as a result the down flow rate decreases to point B. The down flow rate remains almost constant up to an air flow rate marked by point C after which it steadily decreases until it becomes zero at the tube dryout point marked D. The liquid film may be seen as a sub-flooded film between points B and C. This type of behaviour of the down flow rate has not been reported before. To confirm the data, the measurements were carried out again and produced remarkably repeatable results. Noting that the air flow rate for complete dry out of the tube was not the same for all air flow rates, the post-flooding data were replotted in dimensionless form in Fig. 6(b) in terms of dimensionless down flow rate and dimensionless air flow rate defined respectively as

$$\begin{aligned} U^*_{\mathrm{Ld}} &= U_{\mathrm{Ld}}/U_{\mathrm{L}}, \\ U^*_{\mathrm{G}} &= (U_{\mathrm{G}} - U_{\mathrm{G,f}})/(U_{\mathrm{G,do}} - U_{\mathrm{G,f}}), \end{aligned} \tag{1}$$

where U_{Ld} and U_{L} are the down flow rate and input flow rate of liquid, respectively. $U_{\mathrm{G,f}}$ is the gas velocity at flooding point and $U_{\mathrm{G,do}}$ is the gas velocity at complete dry out of the tube. It should be noted that under post-flooding conditions, these dimensionless parameters vary between 0 and 1. The flooding point is represented by the point $(0, 1)$ and the flow reversal point by $(1, 0)$ on this two-dimensional plot. All the data obtained in the 25 mm diameter tube fall roughly on a single curve which has a shape similar to the schematic variation shown in Fig. 6(a). This suggests a possible form of correlating the down flow rate under post-flooding conditions. Such a correlation would require the data for a variety of flow conditions and tube diameters as well as reliable means of predicting the gas flow rate at flooding and at complete tube dryout under the same conditions. Since such data is not available, a correlation is not attempted and is left as possible future work.

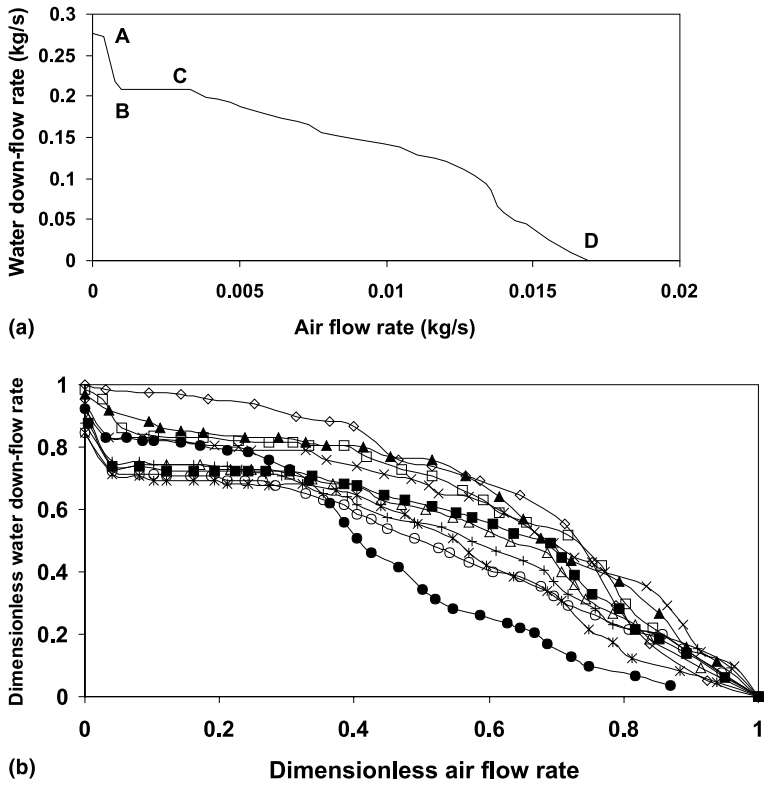

Fig. 6. Water down flow rate in post-flooding region: (a) typical variation with air flow rate; (b) its non-dimensional representation.

4. Correlation for the pressure gradient

Typical variation of the pressure gradient measured in the present study is shown in Figs. 7(a) and (b) where data obtained in the 25 mm and 67 mm tube diameters, respectively, are shown at various liquid flow rates. The pressure gradient typically exhibits a sudden and large increase, by an order of magnitude, following flooding. Such large increases have also been reported by Hewitt et al. (1965) and Dukler and Smith (1982), among others. The pressure gradient remains very high in the post-flooding conditions though eventually it should decrease as the flow reversal point is approached. Another interesting point to note is that the "jump" in the pressure gradient is a strong function of the liquid flow rate and that the jump exists in both 25 and 67 mm diameter tubes and is therefore not specifically associated with a particular mechanism of flooding.

There have been some previous attempts to determine the pressure gradient under flooding and post-flooding conditions. Principal among these are the studies of Bharathan et al. (1978) and Bharathan et al. (1979). They evaluated the pressure gradient in terms of the interfacial friction factor defined as

$$f_{\mathrm{i}} = \frac{\tau_i \alpha^{2.5}}{\frac{1}{2}\rho_{\mathrm{G}} U_{\mathrm{GS}}^2} = \frac{\left(-\frac{\mathrm{d}p}{\mathrm{d}z}\right)\frac{D}{4}\alpha^{2.5}}{\frac{1}{2}\rho_{\mathrm{G}} U_{\mathrm{GS}}^2}, \tag{2}$$

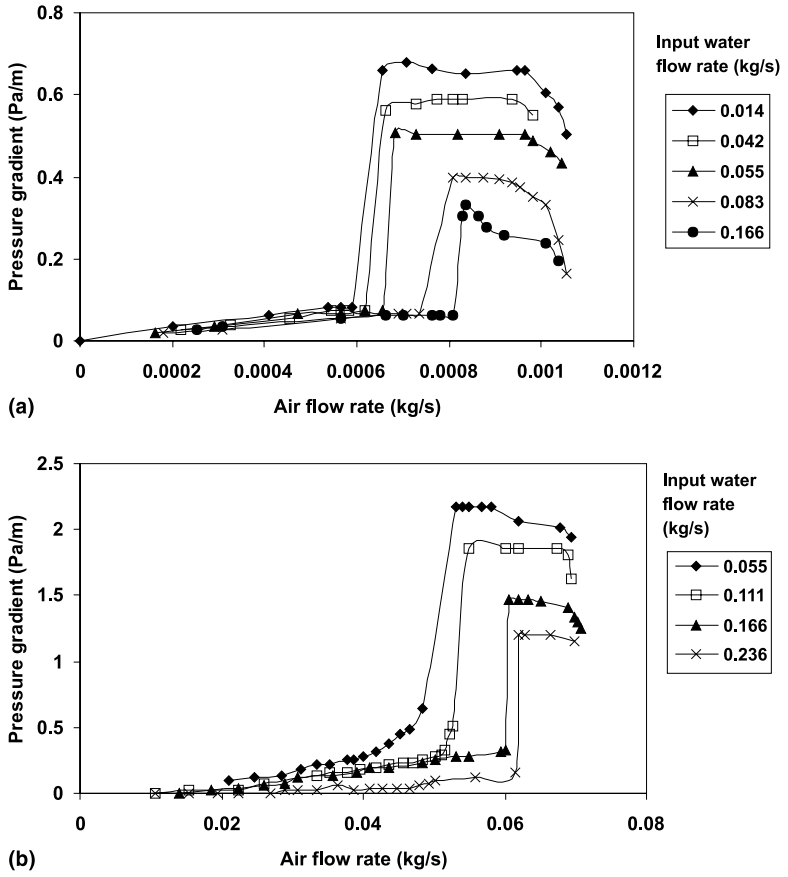

Fig. 7. Variation of the pressure gradient with air flow rate at various water input flow rates in (a) 25 and (b) 67 mm diameter test sections.

where τ_i is the interfacial shear stress and α is void fraction and is related to the film thickness as

$$\alpha = \left(1 - \frac{2\delta}{D}\right)^2. \tag{3}$$

They proposed empirical correlations for f_i to fit their data. In contrast to the above where entirely independent correlations were developed for the interfacial friction factor in countercurrent flow, Richter (1981) proposed a slightly modified form of the Wallis (1969) formula for interfacial friction in annular flow.

A comparison of the performance of the above correlations against data obtained in the present study in 25 and 67 mm diameter tubes and the data reported by Dukler and Smith (1982) in a 50.8 mm diameter tube showed that there was a considerable deviation from the measured friction factor with the predicted value being an order of magnitude less for high values of f_i. At low values of f_i, there was large scatter in the predictions and the average relative error in all the cases is nearly 800%. The principal reason for this disagreement is that

the friction factor obtained in the present study is very high for reasons discussed in the following. Thus, it is clear that a new correlation is required. To this effect, data obtained in the 25 and 67 mm diameter test sections were augmented with the data obtained by Dukler and coworkers in a 50.8 mm diameter test section to create a data bank of 128 points reporting pressure drop under post-flooding conditions in air–water countercurrent flow at atmospheric conditions. These data are used here to construct a correlation for the interfacial friction factor under post-flooding conditions.

The form of the correlation for f_i presented some problems because the present experimental data in countercurrent flow gave a friction factor (obtained using Eq. (2)) which was very high, of the order of unity, in some cases whereas the friction factor even in very rough pipes in single phase flow is only of the order of a small fraction. A closer examination of the data revealed that the unusually high friction factor values corresponded mainly to the post-flooding data in the 25 mm diameter tube. Here the combination of high pressure drop (caused by repeated "slugging" associated with the upward transport of flooding waves within the tube) and the low air velocity at which this happens, especially at high water flow rates, led to very high values of f_i. High values of f_i, of the order of 0.5, have also been reported by Dukler and Smith (1982) in a tube diameter of 50.8 mm and similar values have been obtained in the present study in the 67 mm diameter tube. Thus, the high values of f_i are not an aberration but are characteristic of the interfacial friction under flooding conditions and the correlation developed to predict f_i must take this into account.

It is clear that such high values cannot be accommodated in an equivalent sand grain roughness concept (Schlichting, 1968) because the corresponding sand roughness would be greater than the pipe diameter itself. In all probability, the effective roughness is more representative of the repeated creation, breaking up and entrainment of large waves that goes on under post-flooding conditions rather than of flow over a rough surface. In view of this, it was decided to abandon the concept of equivalent sand grain roughness and develop a correlation in terms of the predominant dimensionless numbers. Since the gas phase fraction, α, has not been measured directly, the interfacial friction factor has been evaluated for annular flow as

$$f_i = \frac{\tau_i}{\frac{1}{2}\rho_G (U_{GS} - U_{LS})^2} \approx \frac{\tau_i}{\frac{1}{2}\rho_G U_{GS}^2}, \tag{4}$$

where U_{GS} and U_{LS} are the superficial velocities of the gas and the liquid phases, respectively. Since the pressure drop varied with both air flow rate and the water flow rate and since the tube diameter and the film thickness were expected to determine to some extent the interfacial interaction, a correlation for f_i was sought in terms of the following dimensionless numbers:

$$f_i = f(Re_L, Re_G, Fr_L, \delta^*, D^*), \tag{5}$$

where Re_L and Re_G are the phasic Reynolds numbers defined based on the superficial velocity and the tube diameter, Fr_L is the liquid phase Froude number defined based on the superficial velocity of the liquid and the tube diameter and $\delta^* = \delta/(\sigma/g\Delta\rho)^{1/2}$ and $D^* = D/(\sigma/g\Delta\rho)^{1/2}$ are the non-dimensional film thickness and the tube diameter used by Bharathan and Wallis (1983). (It should be noted however that all the data used in the correlation were obtained with air and water as the working fluids and except for small changes associated with changes in the test

section pressure, the densities and viscosities of the phases are unaltered. Changes in Re_L and Re_G are brought about only due to changes in velocities and diameters.) Even though the parameter Fr_L was sought to be included in the correlation, the exponent for Fr_L, obtained through multilinear regression, was found to be only 0.025 showing that it had negligible effect. Other possible definitions of Fr_L, defined based on the actual film velocity and the tube diameter or the film thickness were also tried but these again indicated negligible effect of Fr_L on the value of the interfacial friction factor. Substantial exponents for Fr_L could only be obtained when the film thickness term was omitted from the correlation, but this led to poor prediction overall. It was therefore decided to drop the Froude number term from the correlation and seek a correlation of the form

$$f_i = f((Re_L/Re_G), Re_G, \delta/D), \tag{6}$$

which allows the Reynolds numbers to show an independent variation in addition to a joint variation in the form of the loading ratio. However, even this correlation resulted in a small value of the exponent of Re_G and the correlation was ultimately reduced to the following simple form:

$$f_i = f((Re_L/Re_G), \delta/D). \tag{7}$$

Although such a correlation predicted the data well with a regression coefficient of 0.94, there was considerable overprediction of the data at low values of f_i. Given that large f_i are associated with data from the small diameter tube, it may be concluded that this correlation is not very successful in integrating the data from different tube diameters. In view of this, an attempt was made to integrate the data from different diameters by recasting them in terms of observed general variation with each parameter (e.g., f_i increasing with increasing Re_L and δ^*). It was found by trial and error that the data from the different diameters could be made to fall on a single continuous curve if they were replotted as $f_i Re_L^{0.5}$ vs Re_G/δ^* as shown in Fig. 8(a). Using this and after adjusting the exponents for best prediction, the following correlation has been obtained for f_i:

$$f_i = 400\, Re_L^{0.5}\, Re_G^{-1.2}\, D^*\delta^*. \tag{8}$$

The overall performance of this correlation is better than that of Eq. (7) above in that the overall regression coefficient has now increased from 0.94 to 0.96. More significantly, the overprediction at small f_i is now considerably reduced (Fig. 8(b)). It performs well when compared with the experimental values and most of the data, except for a few points, lie within ±30% of the experimental value. There is no systematic error and the average relative error comes down from nearly 800% with existing correlations to 41% with the proposed correlation.

To use the above correlation, it is necessary to know the film thickness under post-flooding conditions. As pointed out earlier, the mean film thickness data under pre-flooding conditions agree well with that predicted by falling film correlations such as those of Nusselt (1916a,b) and Feind (1960). However, under post-flooding conditions, the mean film thickness deviates considerably from the Nusselt theory (Fig. 9). There can be several reasons for this. The decreased film flow rate (due to part of the liquid being taken up by the gas stream) following flooding may lead to a lower film thickness. The formation of large waves on the film may decrease the mean film thickness as compared to that of a smooth film for the same liquid flow rate (Jayanti and Hewitt, 1997). This may again lead to a smaller film thickness under post-flooding conditions. The conductance probes themselves may underestimate the actual film thickness in the presence of

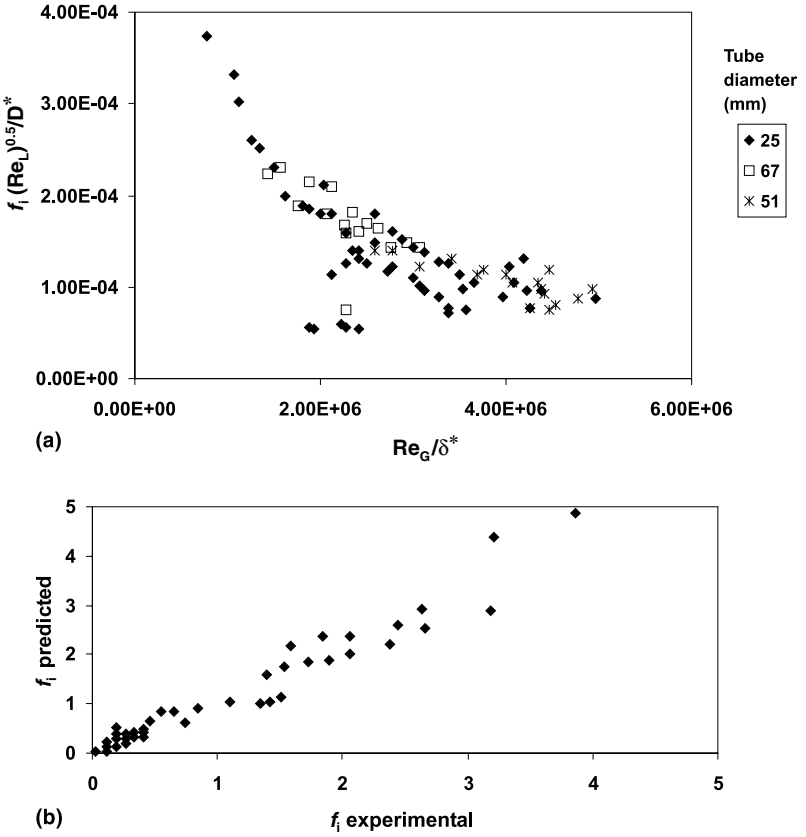

Fig. 8. Correlation of the pressure gradient data: (a) regrouping of data; (b) comparison of the predicted and the experimental value of interfacial friction factor.

large waves (due to probe saturation and loss of sensitivity). Finally, the increased interfacial shear may reduce the average velocity in the liquid film and thereby *increase* the film thickness as compared to the Nusselt film thickness where the interfacial shear is assumed to be zero. Thus, for

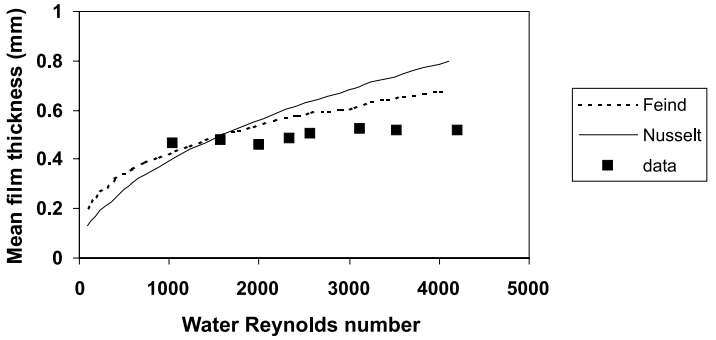

Fig. 9. Variation of mean film thickness under post-flooding conditions in the 67 mm diameter test section.

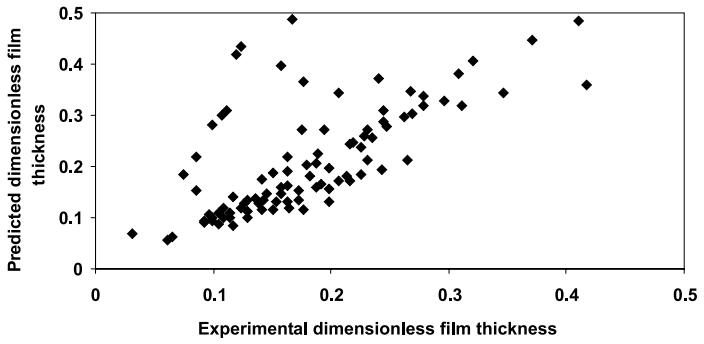

Fig. 10. Comparison of the experimental and predicted value of the dimensionless film thickness.

a variety of factors, the film thickness under post-flooding conditions is different from that given by the Nusselt theory.

In view of this, a correlation is sought for the post-flooding film thickness in dimensionless terms as

$$\delta_{\mathrm{pf}} = f(Re_{\mathrm{L}}, Re_{\mathrm{G},}, \delta^*_{\mathrm{th}}, D^*), \tag{9}$$

where δ_{pf} is the dimensionless post-flooding film thickness, δ^*_{th} is the dimensionless theoretical film thickness and is calculated from the Nusselt theory or from the correlation of Feind (1960) depending on the film Reynolds number. Using regression analysis, the following correlation was obtained:

$$\delta_{\mathrm{pf}} = 2.5\, Re_{\mathrm{L}}^{-0.15}\, Re_{\mathrm{G}}^{0.1}\, D^{*-0.3}\, \delta^*_{\mathrm{th}}. \tag{10}$$

A comparison between the predicted and the experimental film thickness is shown in Fig. 10. Although there is considerable scatter in the correlation, most of the points lie within $\pm 30\%$ and the average relative error is 38%.

The above correlation for the mean film thickness can be used in Eq. (8); the resulting correlation for f_{i} reduces the regression coefficient between the predicted and the experimental f_{i} to 0.91. Therefore, there is a slight loss of correlation, as expected, but the overall prediction remains quite good and the average relative error for the proposed correlation is considerably lesser than the value of about 800% obtained using existing correlations.

5. Conclusions

An experimental study has been conducted to study the post-flooding regime in tubes of 25 and 67 mm internal diameter. Measurements of the pressure gradient in the countercurrent flow section, film thickness near the liquid outlet and the liquid down flow rate were measured over a range of air and water flow rates. It was found that the existing correlations for predicting the pressure drop under flooding conditions gave poor prediction of the current data as well as of the data collected from the literature. Also the film thickness was found to vary significantly from the Nusselt/Feind relations under post-flooding conditions. Hence, new correlations have been

proposed to predict the interfacial friction and the mean film thickness. The down flow rate measurements under post-flooding conditions showed the existence of a sub-critical falling liquid film. A suitable non-dimensionalization of the liquid down flow rate vs air flow rate curve has been suggested.

Acknowledgements

The work described in this paper was carried out as part of a research grant from the Department of Science and Technology, India.

References

Alekseev, V.P., Pobereskin, A.E., Gerasimov, P.V., 1972. Determination of flooding rates in regular packings. Heat Transfer – Soviet Res. 4, 159–163.

Bharathan, D., Wallis, G.B., 1983. Air–water countercurrent annular flow. Int. J. Multiphase Flow 9, 349–366.

Bharathan, D., Wallis, G.B., Richter, H.J., 1978. Air–water countercurrent annular flow. EPRI Report No. NP-786.

Bharathan, D., Wallis, G.B., Richter, H.J., 1979. Air–water countercurrent annular flow. Report No. EPRI-NP-1165, Electric Power Research Institute, Palo Alto, CA.

Clift, R.C., Pritchard, C.L., Nedderman, R.M., 1966. The effect of viscosity on the flooding conditions in wetted wall columns. Chem. Eng. Sci 21, 87–95.

Dukler, A.E., Smith, L, 1982. Two-phase interactions in counter current flow: studies of the flooding mechanism. Annual Report, November 1985–October 1987, NUREG/CR-0617, US Nuclear Regulatory Commission, Washington DC.

Feind, F., 1960. Falling liquid films with countercurrent air flow in vertical tubes. VDI-Forschungsh. 481, 26.

Govan, A.H., Hewitt, G.F., Richter, H.J., Scott, A., 1991. Flooding and churn flow in vertical pipes. Int. J. Multiphase Flow 17, 27–44.

Hewitt, G.F., 1989. Countercurrent two-phase flow invited lecture. In: Fourth Int. Topical Meeting on Nuclear Reactor Thermal Hydraulics, Karlsruhe, Germany.

Hewitt, G.F., Wallis, G.B., 1963. Flooding and associated phenomena in falling film flow in a vertical tube. UKAEA Report, AERE R-4022.

Hewitt, G.F., Lacey, P.M.C., Nicholls, B., 1965. Transitions in film flow in a vertical tube. In: Symp. on Two-phase Flow, Paper B4, Exeter, UK.

Jayanti, S., Hewitt, G.F., 1997. Hydrodynamics and heat transfer of wavy thin film flow. Int. J. Heat Mass Transfer 40, 179–190.

Jayanti, S., Tokarz, A., Hewitt, G.F., 1996. Theoretical investigation of the diameter effect on flooding in countercurrent flow. Int. J. Multiphase Flow 22, 307–324.

McQuillan, K.W., Whalley, P.B., Hewitt, G.F., 1985. Flooding in vertical two-phase flow. Int. J. Multiphase Flow 11, 741–760.

Nusselt, W., 1916a. Surface condensation of water vapour. Z. Ver. D. Ing. 60 (27), 541–546.

Nusselt, W., 1916b. Surface condensation of water vapour. Z. Ver. D. Ing. 60 (26), 569–575.

Pushkina, O.L., Sorokin, Y.L., 1969. Breakdown of liquid film motion in vertical tubes. Heat Transfer – Soviet Res. 1, 56–64.

Richter, H.J., 1981. Flooding in tubes and annuli. Int. J. Multiphase Flow 7, 647–658.

Schlichting, H., 1968. Boundary Layer Theory. McGraw-Hill, New York.

Vijayan, M., Jayanti, S., Balakrishnan, A.R., 2001. Effect of tube diameter on flooding. Int. J. Multiphase Flow 27, 797–816.

Vijayan, M., Indu, C., Jayanti, S., Balakrishnan, A.R., 1999. Circumferential coherence of waves in falling film and the mechanism of flooding in courntercurrent flow. In: Proc. Int. Conf. on Two-phase Flow Modelling and Experimentation. Pisa, Italy, pp. 607–611.

Wallis, G.B., 1969. One Dimensional Two-phase Flow. McGraw-Hill, New York.

Zabaras, G.J., Dukler, A.E., 1988. Countercurrent gas–liquid annular flow including the flooding state. AIChE J. 34, 389–396.